Measurements of the center-of-mass energies of e^+e^- collisions at BESIII*

M. Ablikim[1] M. N. Achasov[10,b] P. Adlarson[67] S. Ahmed[15] M. Albrecht[4] R. Aliberti[28] A. Amoroso[66A,66C] M. R. An[32] Q. An[63,49] X. H. Bai[57] Y. Bai[48] O. Bakina[29] R. Baldini Ferroli[23A] I. Balossino[24A] Y. Ban[38,h] K. Begzsuren[26] N. Berger[28] M. Bertani[23A] D. Bettoni[24A] F. Bianchi[66A,66C] J. Bloms[60] A. Bortone[66A,66C] I. Boyko[29] R. A. Briere[5] H. Cai[68] X. Cai[1,49] A. Calcaterra[23A] G. F. Cao[1,54] N. Cao[1,54] S. A. Cetin[53A] J. F. Chang[1,49] W. L. Chang[1,54] G. Chelkov[29,a] D. Y. Chen[6] G. Chen[1] H. S. Chen[1,54] M. L. Chen[1,49] S. J. Chen[35] X. R. Chen[25] Y. B. Chen[1,49] Z. J. Chen[20,i] W. S. Cheng[66C] G. Cibinetto[24A] F. Cossio[66C] X. F. Cui[36] H. L. Dai[1,49] X. C. Dai[1,54] A. Dbeyssi[15] R. E. de Boer[4] D. Dedovich[29] Z. Y. Deng[1] A. Denig[28] I. Denysenko[29] M. Destefanis[66A,66C] F. De Mori[66A,66C] Y. Ding[33] C. Dong[36] J. Dong[1,49] L. Y. Dong[1,54] M. Y. Dong[1,49,54] X. Dong[68] S. X. Du[71] Y. L. Fan[68] J. Fang[1,49] S. S. Fang[1,54] Y. Fang[1] R. Farinelli[24A] L. Fava[66B,66C] F. Feldbauer[4] G. Felici[23A] C. Q. Feng[63,49] J. H. Feng[50] M. Fritsch[4] C. D. Fu[1] Y. Gao[64] Y. Gao[38,h] Y. Gao[63,49] Y. G. Gao[6] I. Garzia[24A,24B] P. T. Ge[68] C. Geng[50] E. M. Gersabeck[58] A Gilman[61] K. Goetzen[11] L. Gong[33] W. X. Gong[1,49] W. Gradl[28] M. Greco[66A,66C] L. M. Gu[35] M. H. Gu[1,49] Y. T. Gu[13] C. Y Guan[1,54] A. Q. Guo[22] L. B. Guo[34] R. P. Guo[40] Y. P. Guo[9,f] A. Guskov[29,a] T. T. Han[41] W. Y. Han[32] X. Q. Hao[16] F. A. Harris[56] K. L. He[1,54] F. H. Heinsius[4] C. H. Heinz[28] T. Held[4] Y. K. Heng[1,49,54] C. Herold[51] M. Himmelreich[11,d] T. Holtmann[4] G. Y. Hou[1,54] Y. R. Hou[54] Z. L. Hou[1] H. M. Hu[1,54] J. F. Hu[47,j] T. Hu[1,49,54] Y. Hu[1] G. S. Huang[63,49] L. Q. Huang[64] X. T. Huang[41] Y. P. Huang[1] Z. Huang[38,h] T. Hussain[65] N Husken[22,28] W. Ikegami Andersson[67] W. Imoehl[22] M. Irshad[63,49] S. Jaeger[4] S. Janchiv[26] Q. Ji[1] Q. P. Ji[16] X. B. Ji[1,54] X. L. Ji[1,49] Y. Y. Ji[41] H. B. Jiang[41] X. S. Jiang[1,49,54] J. B. Jiao[41] Z. Jiao[18] S. Jin[35] Y. Jin[57] M. Q. Jing[1,54] T. Johansson[67] N. Kalantar-Nayestanaki[55] X. S. Kang[33] R. Kappert[55] M. Kavatsyuk[55] B. C. Ke[43,1] I. K. Keshk[4] A. Khoukaz[60] P. Kiese[28] R. Kiuchi[1] R. Kliemt[11] L. Koch[30] O. B. Kolcu[53A,m] B. Kopf[4] M. Kuemmel[4] M. Kuessner[4] A. Kupsc[67] M. G. Kurth[1,54] W. Kuhn[30] J. J. Lane[58] J. S. Lange[30] P. Larin[15] A. Lavania[21] L. Lavezzi[66A,66C] Z. H. Lei[63,49] H. Leithoff[28] M. Lellmann[28] T. Lenz[28] C. Li[39] C. H. Li[32] Cheng Li[63,49] D. M. Li[71] F. Li[1,49] G. Li[1] H. Li[63,49] H. Li[43] H. B. Li[1,54] H. J. Li[16] J. L. Li[41] J. Q. Li[4] J. S. Li[50] Ke Li[1] L. K. Li[1] Lei Li[3] P. R. Li[31,k,l] S. Y. Li[52] W. D. Li[1,54] W. G. Li[1] X. H. Li[63,49] X. L. Li[41] Xiaoyu Li[1,54] Z. Y. Li[50] H. Liang[1,54] H. Liang[63,49] H. Liang[27] Y. F. Liang[45] Y. T. Liang[25] G. R. Liao[12] L. Z. Liao(廖龙洲)[1,54†] J. Libby[21] C. X. Lin[50] B. J. Liu[1] C. X. Liu[1] D. Liu[15,63] F. H. Liu[44] Fang Liu[1] Feng Liu[6] H. B. Liu[13] H. M. Liu[1,54] Huanhuan Liu[1] Huihui Liu[17] J. B. Liu[63,49] J. L. Liu[64] J. Y. Liu[1,54] K. Liu[1] K. Y. Liu[33] L. Liu[63,49] M. H. Liu[9,f] P. L. Liu[1] Q. Liu[54] Q. Liu[68] S. B. Liu[63,49] Shuai Liu[46] T. Liu[1,54] W. M. Liu[63,49] X. Liu[31,k,l] Y. Liu[31,k,l] Y. B. Liu[36] Z. A. Liu[1,49,54] Z. Q. Liu[41] X. C. Lou[1,49,54] F. X. Lu[50] H. J. Lu[18] J. D. Lu[1,54] J. G. Lu[1,49] X. L. Lu[1] Y. Lu[1] Y. P. Lu[1,49] C. L. Luo[34] M. X. Luo[70] P. W. Luo[50] T. Luo[9,f] X. L. Luo[1,49] X. R. Lyu[54] F. C. Ma[33] H. L. Ma[1] L. L. Ma[41] M. M. Ma[1,54] Q. M. Ma[1] R. Q. Ma[1,54] R. T. Ma[54] X. X. Ma[1,54] X. Y. Ma[1,49] F. E. Maas[15] M. Maggiora[66A,66C]

Received 29 December 2020; Accepted 19 July 2021; Published online 18 August 2021

* Supported in part by National Key Research and Development Program of China (2020YFA0406300, 2020YFA0406400); National Natural Science Foundation of China (NSFC) (11625523, 11635010, 11735014, 11822506, 11835012, 11935015, 11935016, 11935018, 11961141012); the Chinese Academy of Sciences (CAS) Large-Scale Scientific Facility Program; Joint Large-Scale Scientific Facility Funds of the NSFC and CAS (U1732263, U1832207); CAS Key Research Program of Frontier Sciences (QYZDJ-SSW-SLH003, QYZDJ-SSW-SLH040); 100 Talents Program of CAS; INPAC and Shanghai Key Laboratory for Particle Physics and Cosmology; ERC (758462); European Union Horizon 2020 research and innovation programme (Marie Sklodowska-Curie grant agreement No 894790); German Research Foundation DFG (443159800), Collaborative Research Center CRC 1044, FOR 2359, FOR 2359, GRK 214; Istituto Nazionale di Fisica Nucleare, Italy; Ministry of Development of Turkey (DPT2006K-120470); National Science and Technology fund; Olle Engkvist Foundation (200-0605); STFC (United Kingdom); The Knut and Alice Wallenberg Foundation (Sweden) (2016.0157); The Royal Society, UK (DH140054, DH160214); The Swedish Research Council; U. S. Department of Energy (DE-FG02-05ER41374, DE-SC-0012069)

† E-mail: liaolz@ihep.ac.cn

S. Maldaner[4] S. Malde[61] Q. A. Malik[65] A. Mangoni[23B] Y. J. Mao[38,h] Z. P. Mao[1] S. Marcello[66A,66C] Z. X. Meng[57] J. G. Messchendorp[55] G. Mezzadri[24A] T. J. Min[35] R. E. Mitchell[22] X. H. Mo[1,49,54] N. Yu. Muchnoi[10,b] H. Muramatsu[59] S. Nakhoul[11,d] Y. Nefedov[29] F. Nerling[11,d] I. B. Nikolaev[10,b] Z. Ning[1,49] S. Nisar[8,g] S. L. Olsen[54] Q. Ouyang[1,49,54] S. Pacetti[23B,23C] X. Pan[9,f] Y. Pan[58] A. Pathak[1] A. Pathak[27] P. Patteri[23A] M. Pelizaeus[4] H. P. Peng[63,49] K. Peters[11,d] J. Pettersson[67] J. L. Ping[34] R. G. Ping[1,54] S. Pogodin[29] R. Poling[59] V. Prasad[63,49] H. Qi[63,49] H. R. Qi[52] K. H. Qi[25] M. Qi[35] T. Y. Qi[9] S. Qian[1,49] W. B. Qian[54] Z. Qian[50] C. F. Qiao[54] L. Q. Qin[12] X. P. Qin[9] X. S. Qin[41] Z. H. Qin[1,49] J. F. Qiu[1] S. Q. Qu[36] K. H. Rashid[65] K. Ravindran[21] C. F. Redmer[28] A. Rivetti[66C] V. Rodin[55] M. Rolo[66C] G. Rong[1,54] Ch. Rosner[15] M. Rump[60] H. S. Sang[63] A. Sarantsev[29,c] Y. Schelhaas[28] C. Schnier[4] K. Schoenning[67] M. Scodeggio[24A,24B] D. C. Shan[46] W. Shan[19] X. Y. Shan[63,49] J. F. Shangguan[46] M. Shao[63,49] C. P. Shen[9] H. F. Shen[1,54] P. X. Shen[36] X. Y. Shen[1,54] H. C. Shi[63,49] R. S. Shi[1,54] X. Shi[1,49] X. D Shi[63,49] J. J. Song[41] W. M. Song[27,1] Y. X. Song[38,h] S. Sosio[66A,66C] S. Spataro[66A,66C] K. X. Su[68] P. P. Su[46] F. F. Sui[41] G. X. Sun[1] H. K. Sun[1] J. F. Sun[16] L. Sun[68] S. S. Sun[1,54] T. Sun[1,54] W. Y. Sun[34] W. Y. Sun[27] X Sun[20,i] Y. J. Sun[63,49] Y. K. Sun[63,49] Y. Z. Sun[1] Z. T. Sun[1] Y. H. Tan[68] Y. X. Tan[63,49] C. J. Tang[45] G. Y. Tang[1] J. Tang[50] J. X. Teng[63,49] V. Thoren[67] W. H. Tian[43] Y. T. Tian[25] I. Uman[53B] B. Wang[1] C. W. Wang[35] D. Y. Wang[38,h] H. J. Wang[31,k,l] H. P. Wang[1,54] K. Wang[1,49] L. L. Wang[1] M. Wang[41] M. Z. Wang[38,h] Meng Wang[1,54] W. Wang[50] W. H. Wang[68] W. P. Wang[63,49] X. Wang[38,h] X. F. Wang[31,k,l] X. L. Wang[9,f] Y. Wang[50] Y. Wang[63,49] Y. D. Wang[37] Y. F. Wang[1,49,54] Y. Q. Wang[1] Y. Y. Wang[31,k,l] Z. Wang[1,49] Z. Y. Wang[1] Ziyi Wang[54] Zongyuan Wang[1,54] D. H. Wei[12] F. Weidner[60] S. P. Wen[1] D. J. White[58] U. Wiedner[4] G. Wilkinson[61] M. Wolke[67] L. Wollenberg[4] J. F. Wu[1,54] L. H. Wu[1] L. J. Wu[1,54] X. Wu[9,f] Z. Wu[1,49] L. Xia[63,49] H. Xiao[9,f] S. Y. Xiao[1] Z. J. Xiao[34] X. H. Xie[38,h] Y. G. Xie[1,49] Y. H. Xie[6] T. Y. Xing[1,54] G. F. Xu[1] Q. J. Xu[14] W. Xu[1,54] X. P. Xu[46] Y. C. Xu[54] F. Yan[9,f] L. Yan[9,f] W. B. Yan[63,49] W. C. Yan[71] Xu Yan[46] H. J. Yang[42,e] H. X. Yang[1] L. Yang[43] S. L. Yang[54] Y. X. Yang[12] Yifan Yang[1,54] Zhi Yang[25] M. Ye[1,49] M. H. Ye[7] J. H. Yin[1] Z. Y. You[50] B. X. Yu[1,49,54] C. X. Yu[36] G. Yu[1,54] J. S. Yu[20,i] T. Yu[64] C. Z. Yuan(苑长征)[1,54] L. Yuan[2] X. Q. Yuan[38,h] Y. Yuan[1] Z. Y. Yuan[50] C. X. Yue[32] A. A. Zafar[65] X. Zeng Zeng[6] Y. Zeng[20,i] A. Q. Zhang[1] B. X. Zhang[1] Guangyi Zhang[16] H. Zhang[63] H. H. Zhang[27] H. H. Zhang[50] H. Y. Zhang[1,49] J. J. Zhang[43] J. L. Zhang[69] J. Q. Zhang[34] J. W. Zhang[1,49,54] J. Y. Zhang[1] J. Z. Zhang[1,54] Jianyu Zhang[1,54] Jiawei Zhang[1,54] L. M. Zhang[52] L. Q. Zhang[50] Lei Zhang[35] S. Zhang[50] S. F. Zhang[35] Shulei Zhang[20,i] X. D. Zhang[37] X. Y. Zhang[41] Y. Zhang[61] Y. T. Zhang[71] Y. H. Zhang[1,49] Yan Zhang[63,49] Yao Zhang[1] Z. Y. Zhang[68] G. Zhao[1] J. Zhao[32] J. Y. Zhao[1,54] J. Z. Zhao[1,49] Lei Zhao[63,49] Ling Zhao[1] M. G. Zhao[36] Q. Zhao[1] S. J. Zhao[71] Y. B. Zhao[1,49] Y. X. Zhao[25] Z. G. Zhao[63,49] A. Zhemchugov[29,a] B. Zheng[64] J. P. Zheng[1,49] Y. H. Zheng[54] B. Zhong[34] C. Zhong[64] L. P. Zhou[1,54] Q. Zhou[1,54] X. Zhou[68] X. K. Zhou[54] X. R. Zhou[63,49] X. Y. Zhou[32] A. N. Zhu[1,54] J. Zhu[36] K. Zhu[1] K. J. Zhu[1,49,54] S. H. Zhu[62] T. J. Zhu[69] W. J. Zhu[9,f] W. J. Zhu[36] Y. C. Zhu[63,49] Z. A. Zhu[1,54] B. S. Zou[1] J. H. Zou[1]

(BESIII Collaboration)

[1]Institute of High Energy Physics, Beijing 100049, China
[2]Beihang University, Beijing 100191, China
[3]Beijing Institute of Petrochemical Technology, Beijing 102617, China
[4]Bochum Ruhr-University, D-44780 Bochum, Germany
[5]Carnegie Mellon University, Pittsburgh, Pennsylvania 15213, USA
[6]Central China Normal University, Wuhan 430079, China
[7]China Center of Advanced Science and Technology, Beijing 100190, China
[8]COMSATS University Islamabad, Lahore Campus, Defence Road, Off Raiwind Road, 54000 Lahore, Pakistan
[9]Fudan University, Shanghai 200443, China
[10]G.I. Budker Institute of Nuclear Physics SB RAS (BINP), Novosibirsk 630090, Russia
[11]GSI Helmholtzcentre for Heavy Ion Research GmbH, D-64291 Darmstadt, Germany
[12]Guangxi Normal University, Guilin 541004, China
[13]Guangxi University, Nanning 530004, China
[14]Hangzhou Normal University, Hangzhou 310036, China
[15]Helmholtz Institute Mainz, Staudinger Weg 18, D-55099 Mainz, Germany
[16]Henan Normal University, Xinxiang 453007, China

[17]Henan University of Science and Technology, Luoyang 471003, China
[18]Huangshan College, Huangshan 245000, China
[19]Hunan Normal University, Changsha 410081, China
[20]Hunan University, Changsha 410082, China
[21]Indian Institute of Technology Madras, Chennai 600036, India
[22]Indiana University, Bloomington, Indiana 47405, USA
[23]INFN Laboratori Nazionali di Frascati, (A)INFN Laboratori Nazionali di Frascati, I-00044, Frascati, Italy; (B)INFN Sezione di Perugia, I-06100, Perugia, Italy; (C)University of Perugia, I-06100, Perugia, Italy
[24]INFN Sezione di Ferrara, (A)INFN Sezione di Ferrara, I-44122, Ferrara, Italy; (B)University of Ferrara, I-44122, Ferrara, Italy
[25]Institute of Modern Physics, Lanzhou 730000, China
[26]Institute of Physics and Technology, Peace Ave. 54B, Ulaanbaatar 13330, Mongolia
[27]Jilin University, Changchun 130012, China
[28]Johannes Gutenberg University of Mainz, Johann-Joachim-Becher-Weg 45, D-55099 Mainz, Germany
[29]Joint Institute for Nuclear Research, 141980 Dubna, Moscow region, Russia
[30]Justus-Liebig-Universitaet Giessen, II. Physikalisches Institut, Heinrich-Buff-Ring 16, D-35392 Giessen, Germany
[31]Lanzhou University, Lanzhou 730000, China
[32]Liaoning Normal University, Dalian 116029, China
[33]Liaoning University, Shenyang 110036, China
[34]Nanjing Normal University, Nanjing 210023, China
[35]Nanjing University, Nanjing 210093, China
[36]Nankai University, Tianjin 300071, China
[37]North China Electric Power University, Beijing 102206, China
[38]Peking University, Beijing 100871, China
[39]Qufu Normal University, Qufu 273165, China
[40]Shandong Normal University, Jinan 250014, China
[41]Shandong University, Jinan 250100, China
[42]Shanghai Jiao Tong University, Shanghai 200240, China
[43]Shanxi Normal University, Linfen 041004, China
[44]Shanxi University, Taiyuan 030006, China
[45]Sichuan University, Chengdu 610064, China
[46]Soochow University, Suzhou 215006, China
[47]South China Normal University, Guangzhou 510006, China
[48]Southeast University, Nanjing 211100, China
[49]State Key Laboratory of Particle Detection and Electronics, Beijing 100049, Hefei 230026, China
[50]Sun Yat-Sen University, Guangzhou 510275, China
[51]Suranaree University of Technology, University Avenue 111, Nakhon Ratchasima 30000, Thailand
[52]Tsinghua University, Beijing 100084, China
[53]Turkish Accelerator Center Particle Factory Group, (A)Istanbul Bilgi University, HEP Res. Cent., 34060 Eyup, Istanbul, Turkey; (B)Near East University, Nicosia, North Cyprus, Mersin 10, Turkey
[54]University of Chinese Academy of Sciences, Beijing 100049, China
[55]University of Groningen, NL-9747 AA Groningen, The Netherlands
[56]University of Hawaii, Honolulu, Hawaii 96822, USA
[57]University of Jinan, Jinan 250022, China
[58]University of Manchester, Oxford Road, Manchester, M13 9PL, United Kingdom
[59]University of Minnesota, Minneapolis, Minnesota 55455, USA
[60]University of Muenster, Wilhelm-Klemm-Str. 9, 48149 Muenster, Germany
[61]University of Oxford, Keble Rd, Oxford, UK OX13RH
[62]University of Science and Technology Liaoning, Anshan 114051, China
[63]University of Science and Technology of China, Hefei 230026, China
[64]University of South China, Hengyang 421001, China
[65]University of the Punjab, Lahore-54590, Pakistan
[66]University of Turin and INFN, (A)University of Turin, I-10125, Turin, Italy; (B)University of Eastern Piedmont, I-15121, Alessandria, Italy; (C)INFN, I-10125, Turin, Italy
[67]Uppsala University, Box 516, SE-75120 Uppsala, Sweden
[68]Wuhan University, Wuhan 430072, China
[69]Xinyang Normal University, Xinyang 464000, China
[70]Zhejiang University, Hangzhou 310027, China
[71]Zhengzhou University, Zhengzhou 450001, China
[a]Also at the Moscow Institute of Physics and Technology, Moscow 141700, Russia
[b]Also at the Novosibirsk State University, Novosibirsk, 630090, Russia
[c]Also at the NRC "Kurchatov Institute", PNPI, 188300, Gatchina, Russia
[d]Also at Goethe University Frankfurt, 60323 Frankfurt am Main, Germany
[e]Also at Key Laboratory for Particle Physics, Astrophysics and Cosmology, Ministry of Education; Shanghai Key Laboratory for Particle Physics and Cosmology; Institute of Nuclear and Particle Physics, Shanghai 200240, China
[f]Also at Key Laboratory of Nuclear Physics and Ion-beam Application (MOE) and Institute of Modern Physics, Fudan University, Shanghai 200443, China
[g]Also at Harvard University, Department of Physics, Cambridge, MA, 02138, USA
[h]Also at State Key Laboratory of Nuclear Physics and Technology, Peking University, Beijing 100871, China

[i]Also at School of Physics and Electronics, Hunan University, Changsha 410082, China
[j]Also at Guangdong Provincial Key Laboratory of Nuclear Science, Institute of Quantum Matter, South China Normal University, Guangzhou 510006, China
[k]Also at Frontiers Science Center for Rare Isotopes, Lanzhou University, Lanzhou 730000, China
[l]Also at Lanzhou Center for Theoretical Physics, Lanzhou University, Lanzhou 730000, China
[m]Currently at Istinye University, 34010 Istanbul, Turkey

Abstract: During the 2016-17 and 2018-19 running periods, the BESIII experiment collected 7.5 fb^{-1} of e^+e^- collision data at center-of-mass energies ranging from 4.13 to 4.44 GeV. These data samples are primarily used for the study of excited charmonium and charmoniumlike states. By analyzing the di-muon process $e^+e^- \to (\gamma_{\rm ISR/FSR})\mu^+\mu^-$, we measure the center-of-mass energies of the data samples with a precision of 0.6 MeV. Through a run-by-run study, we find that the center-of-mass energies were stable throughout most of the data-collection period.

Keywords: center-of-mass energy, e^+e^- annihilation, BESIII

DOI: 10.1088/1674-1137/ac1575

I. INTRODUCTION

The BESIII experiment [1] was designed to study physics in the τ-charm energy region (2.0 – 4.9 GeV) [2] through e^+e^- annihilations produced by the BEPCII storage ring [3]. Since it started running in 2008, a variety of data samples have been collected at different center-of-mass (CM) energies for the study of light hadron spectroscopy, charmonium and charmoniumlike states (also called *XYZ* states), charm physics, τ physics, various QCD-related studies, and the search for new physics beyond the standard model [4].

The Beam Energy Measurement System (BEMS) [5] was designed to precisely measure BESIII CM energies ($E_{\rm cm}$) using a method based on Compton back-scattered photons. However, its capability at high energy ($E_{\rm cm}$ above 4 GeV) is degraded by its detection efficiency and limited calibration sources for high-energy gamma rays. Therefore, an alternative algorithm was developed to measure the $E_{\rm cm}$ for data samples above 4 GeV. This method uses the well-understood QED process $e^+e^- \to (\gamma_{\rm ISR/FSR})\mu^+\mu^-$ (the di-muon process), where $\gamma_{\rm ISR/FSR}$ is a radiative photon due to initial state radiation (ISR) and/or final state radiation (FSR). Using this method, a precision of 0.8 MeV was previously achieved for data from 2011 to 2014 [6].

In this paper, we present the $E_{\rm cm}$ measurement for the *XYZ* data samples taken at BESIII from 2017 to 2019. The method used in Ref. [6] is followed, but the precision of the momentum calibration is improved, and the $E_{\rm cm}$ is measured with an uncertainty of 0.6 MeV.

Using the selected di-muon events, $e^+e^- \to (\gamma_{\rm ISR/FSR})\mu^+\mu^-$, we determine $E_{\rm cm}$ using

$$E_{\rm cm} = (M_{\rm p}(\mu^+\mu^-) + \Delta M_{\rm ISR/FSR} + \Delta M_{\rm cal}) \times c^2, \qquad (1)$$

where $M_{\rm p}(\mu^+\mu^-)$ is the peak position of the $\mu^+\mu^-$ invariant mass of selected di-muon events; $\Delta M_{\rm ISR/FSR}$ is the mass shift due to the emission of ISR or FSR photons, estimated from Monte Carlo (MC) simulation of the di-muon process by turning the ISR/FSR processes on and off in MC generation; and $\Delta M_{\rm cal}$ is the correction introduced by the momentum calibration of the $\mu^+\mu^-$ tracks, obtained from an analysis of the process $e^+e^- \to \gamma_{\rm ISR}J/\psi$.

II. THE BESIII DETECTOR AND DATA SETS

The BESIII detector is described in detail in Ref. [1]. The cylindrical core of the detector covers 93% of the full solid angle and consists of a helium-based multilayer drift chamber (MDC), a plastic scintillator time-of-flight system (TOF), and a CsI(Tl) electromagnetic calorimeter (EMC), all of which are enclosed in a superconducting solenoidal magnet providing a 1.0 T magnetic field. The solenoid is supported by an octagonal flux-return yoke with resistive plate counter muon identification modules interleaved with steel. The charged-particle momentum resolution at 1 GeV/c is 0.5, and the dE/dx resolution is 6% for electrons from Bhabha scattering. The EMC measures photon energies with a resolution of 2.5% (5%) at 1 GeV in the barrel (end cap) region. The time resolution in the TOF barrel region is 68 ps, and that in the end cap region is 60 ps [7-9].

The data samples analyzed in this work are listed in Table 1. They include 16 different CM energies from 4.13 to 4.44 GeV and were collected in two running years: from December 2016 to May 2017 (labelled as "2017XYZ" hereafter, the integrated luminosities are measured using the Bhabha events in Ref. [10]) and from February 2019 to June 2019 (labelled as "2019XYZ" hereafter, the integrated luminosities are estimated by using online monitoring information). The column "Sample" lists the nominal CM energy in MeV used during online data collecting. The true CM energy is generally within a few MeV of the nominal value. Run numbers are used to divide the data into subsamples. Other

Table 1. Summary of the data samples, including run numbers, integrated luminosity $\mathcal{L}$ [10], the measured J/ψ mass after FSR correction $M^{\rm cor}(J/\psi)$ (in MeV/c^2), $M_{\rm p}(\mu^+\mu^-)$ (in MeV/c^2), and $E_{\rm cm}$. Superscripts represent data from different periods: "1" denotes 2017XYZ data, and "2" denotes 2019XYZ data. The first uncertainties are statistical and the second systematic.

Sample	Run Number	$\mathcal{L}$/pb^{-1}	$M^{\rm cor}(J/\psi)$	$M_{\rm p}(\mu^+\mu^-)$	$E_{\rm cm}$/MeV
4130^2	59163-59573	400	3100.55 ± 0.30	4130.23 ± 0.05	$4128.78\pm0.05\pm0.36$
4160^2	59574-59896	400	3100.18 ± 0.29	4158.89 ± 0.05	$4157.83\pm0.05\pm0.34$
4190^1	47543-48170	526.70 ± 2.16	3097.89 ± 0.28	4187.90 ± 0.05	$4189.12\pm0.05\pm0.34$
4200^1	48172-48713	526.60 ± 2.05	3098.17 ± 0.27	4198.20 ± 0.05	$4199.15\pm0.05\pm0.34$
4210^1	48714-49239	517.10 ± 1.81	3097.41 ± 0.29	4207.67 ± 0.06	$4209.39\pm0.06\pm0.34$
4220^1	49270-49787	514.60 ± 1.80	3097.51 ± 0.26	4217.31 ± 0.05	$4218.93\pm0.06\pm0.32$
4237^1	49788-50254	530.30 ± 2.39	3097.36 ± 0.24	4233.99 ± 0.04	$4235.77\pm0.04\pm0.30$
4246^1	50255-50793	538.10 ± 2.69	3097.35 ± 0.24	4242.18 ± 0.04	$4243.97\pm0.04\pm0.30$
4270^1	50796-51302	531.10 ± 3.13	3098.09 ± 0.26	4265.74 ± 0.04	$4266.81\pm0.04\pm0.32$
4280^1	51305-51498	175.70 ± 0.97	3097.55 ± 0.48	4277.73 ± 0.04	$4277.78\pm0.11\pm0.52$
4290^2	59902-60363	500	3100.07 ± 0.28	4289.33 ± 0.06	$4288.43\pm0.06\pm0.34$
4315^2	60364-60805	500	3099.97 ± 0.30	4313.46 ± 0.06	$4312.68\pm0.06\pm0.35$
4340^2	60808-61242	500	3099.71 ± 0.29	4338.45 ± 0.06	$4337.93\pm0.06\pm0.35$
4380^2	61249-61762	500	3099.68 ± 0.30	4378.35 ± 0.06	$4377.88\pm0.06\pm0.35$
4400^2	61763-62285	500	3100.61 ± 0.31	4398.21 ± 0.06	$4396.83\pm0.06\pm0.36$
4440^2	62286-62823	570	3099.73 ± 0.29	4437.59 ± 0.06	$4437.10\pm0.06\pm0.35$

columns, such as $\mathcal{L}$ (pb^{-1}), are illustrated below.

A GEANT4 [11] based detector simulation package is developed to model the detector response for MC events. In our analysis, the di-muon sample is generated with BABAYAGA3.5 [12], and the $e^+e^-\to\gamma_{\rm ISR}J/\psi$ sample is generated with KKMC [13, 14]. One million events are generated for each process at each CM energy.

III. EVENT SELECTION AND MEASUREMENT OF $M_p(\mu^+\mu^-)$

The di-muon process $e^+e^-\to(\gamma_{\rm ISR/FSR})\mu^+\mu^-$ is selected by requiring two oppositely charged tracks in the detector, each positively identified as a muon. Both charged tracks are reconstructed from hits in the MDC within the polar angle range $|\cos\theta|<0.8$ and their extrapolations to the interaction point (IP) within 10 cm along the beam direction and 1 cm in the plane perpendicular to the beam. The energy deposition in the EMC for each charged track is required to be less than 0.4 GeV to suppress backgrounds from radiative Bhabha events.

The sample after these selections includes di-muon events with no photon emission or with very low-energy radiative photons, ISR J/ψ with $J/\psi\to\mu^+\mu^-$, and ISR $\mu^+\mu^-$ events with a smooth $\mu^+\mu^-$ invariant mass ($M(\mu^+\mu^-)$) distribution. The events in the J/ψ mass region are used for track momentum calibration and those with high invariant mass are used to measure the $E_{\rm cm}$ after additional selection criteria are applied, as described below.

To suppress di-muon events with high energy radiative photons, a requirement on the cosine of the opening angle between the two tracks, $\cos\theta_{\mu^+\mu^-}<-0.9997$ is applied. To further remove cosmic ray events, the TOF time difference between the two tracks is required to be $|\Delta t|<2$ ns. The background contribution after these selection criteria is less than 0.1% compared with the signal and is therefore neglected in the following analysis.

The $M(\mu^+\mu^-)$ distribution for the 4190 data sample is shown in Fig. 1 as an example. The distributions of the other samples are very similar. The distribution is a Gaussian due to the momentum resolution of the $\mu^+\mu^-$, though it is distorted by ISR and FSR effects, producing a tail on

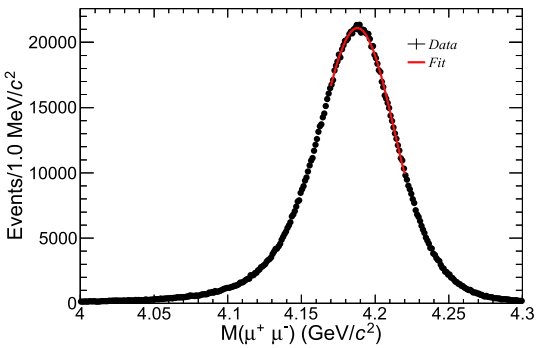

Fig. 1. (color online) The $\mu^+\mu^-$ invariant mass distribution and the fit result of the 4190 sample. Dots with error bars are data, and the solid red curve is the fit.

the left side of the peak. The central part of the distribution can be approximated with a Gaussian function. We measure the peak position of the distribution ($M_{\rm p}(\mu^+\mu^-)$) by fitting it with a Gaussian function in the range of $(-1\sigma, +1.5\sigma)$ around the peak, where σ is the standard deviation of the Gaussian. If the goodness of the fit, $\chi^2/ndf > 2.0$ (ndf is the number of degrees of freedom of the fit), the fit range is slightly reduced until $\chi^2/ndf < 2.0$, guaranteeing a good fit quality. The fit result for the 4190 data sample is shown in Fig. 1. The values of $M_{\rm p}(\mu^+\mu^-)$ for the other data samples are obtained using a similar method and are listed in Table 1.

To examine the stability of the $E_{\rm cm}$ over the data-taking period for each data sample, the fit procedure is repeated for each run of the data sample. The measured peak values of the $\mu^+\mu^-$ invariant mass distribution versus run number for all 16 samples are shown in Fig. 2. There are small jumps of less than 1 MeV in the 4130, 4200, 4210, 4246, 4380, and 4400 samples. Before and after the jumps, the energy is stable. We fit each stable part of the distribution with a linear function and Table 2 summarizes the average, $M^{\rm ave}(\mu^+\mu^-)$, for each period of time. The deviation of $M^{\rm ave}(\mu^+\mu^-)$ from the peak position obtained in the full data sample is considered as one source of systematic uncertainty.

IV. MOMENTUM CALIBRATION WITH ISR J/ψ SIGNAL

The momentum measurement of the muon tracks is validated with $J/\psi \to \mu^+\mu^-$ candidates produced via the process $e^+e^- \to \gamma_{\rm ISR}J/\psi$ selected in the previous section. The distribution of $M(\mu^+\mu^-)$ for each sample is fitted with a crystal-ball function [15] for the J/ψ signal and a linear function to model the background from continuum production of $e^+e^- \to \gamma\mu^+\mu^-$. Figure 3(a) shows the fit result for the 4190 data sample as an example. The peak position of the J/ψ signal, $M^{\rm obs}(J/\psi)$, is used to calibrate the momentum measurement of the muon tracks.

Due to FSR, $J/\psi \to \mu^+\mu^-\gamma_{\rm FSR}$, the measured $M^{\rm obs}(J/\psi)$ is slightly lower than the world average J/ψ mass ($m_{J/\psi}$) given by the PDG [16]. The mass shift due to the FSR photon(s) $\Delta M^{\gamma J/\psi}_{\rm FSR}$ of the process $e^+e^- \to \gamma_{\rm ISR}J/\psi$ at each $E_{\rm cm}$ is obtained by using the generator PHOTOS [17] with FSR turned on or off. The shift is around 0.3 MeV/c^2 with minimal dependence on the CM energy of the data sample.

Comparing the $M^{\rm cor}(J/\psi) = M^{\rm obs}(J/\psi) + \Delta M^{\gamma J/\psi}_{\rm FSR}$ (as shown in Table 1) with the world-average J/ψ mass value $m_{J/\psi}$ in the Particle Data Book (PDG), we measure the bias in the J/ψ mass measurement ($\Delta M^{\rm cor}(J/\psi)$) due to the

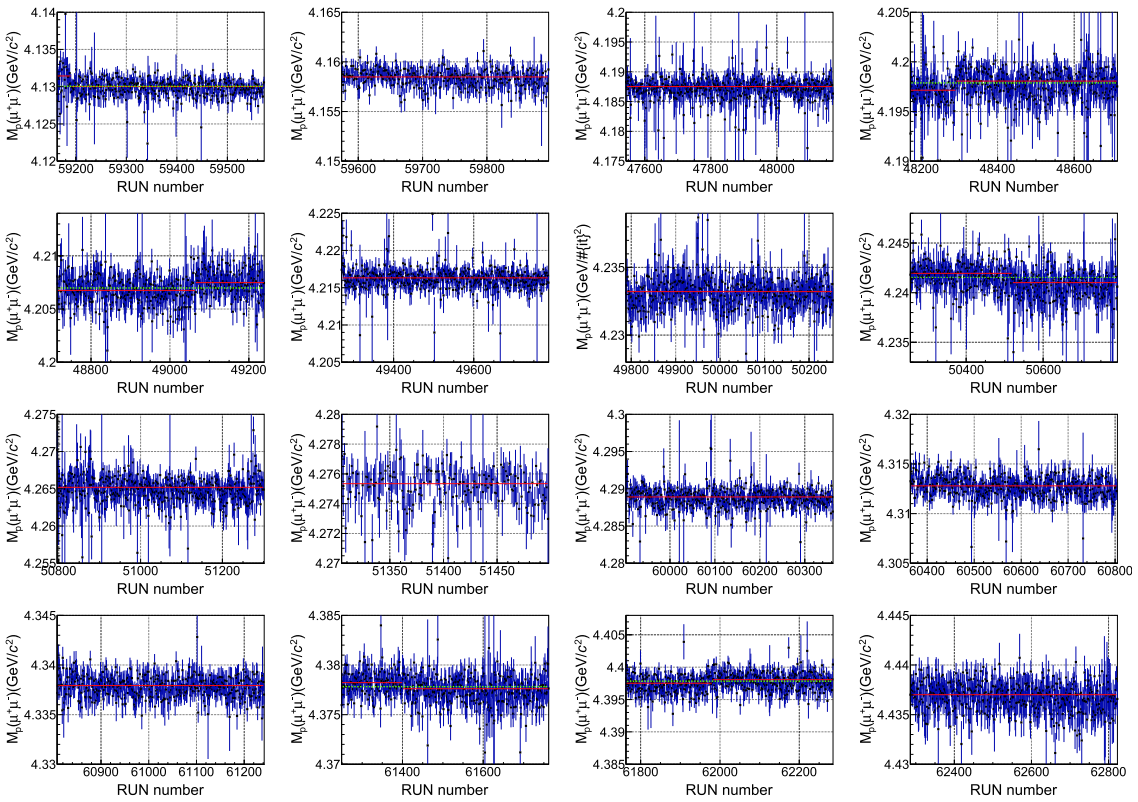

Fig. 2. (color online) Measured run-by-run values for the $M_{\rm p}(\mu^+\mu^-)$ of di-muon events in each data sample. The red solid lines show the fit results for the data samples of each stable period of time. The green dotted lines are the fit results of the entire sample when there is an energy jump.

Table 2. Average value $M^{\rm ave}(\mu^+\mu^-)$ (in MeV/c^2) for each stable data-taking period within each data sample.

Sample	Run Number	$M^{\rm ave}(\mu^+\mu^-)$	Run Number	$M^{\rm ave}(\mu^+\mu^-)$
4130	59163-59190	4131.44 ± 0.36	59191-59573	4130.02 ± 0.05
4160	59574-59896			4158.49 ± 0.05
4190	47543-48170			4187.52 ± 0.06
4200	48172-48290	4197.14 ± 0.12	48291-48713	4198.07 ± 0.06
4210	48174-49065	4206.75 ± 0.06	49066-49239	4207.49 ± 0.09
4220	49270-49787			4216.33 ± 0.05
4237	49788-50254			4233.21 ± 0.04
4246	50255-50520	4241.01 ± 0.08	50521-50793	4241.55 ± 0.05
4270	50796-51302			4265.20 ± 0.06
4280	51305-51498			4275.34 ± 0.09
4290	59902-60363			4288.91 ± 0.05
4315	60364-60805			4312.79 ± 0.04
4340	60808-61242			4337.93 ± 0.05
4380	61249-61400	4378.23 ± 0.09	61401-61762	4377.61 ± 0.06
4400	61763-61980	4397.51 ± 0.08	61981-62285	4398.06 ± 0.07
4440	62286-62823			4437.01 ± 0.05

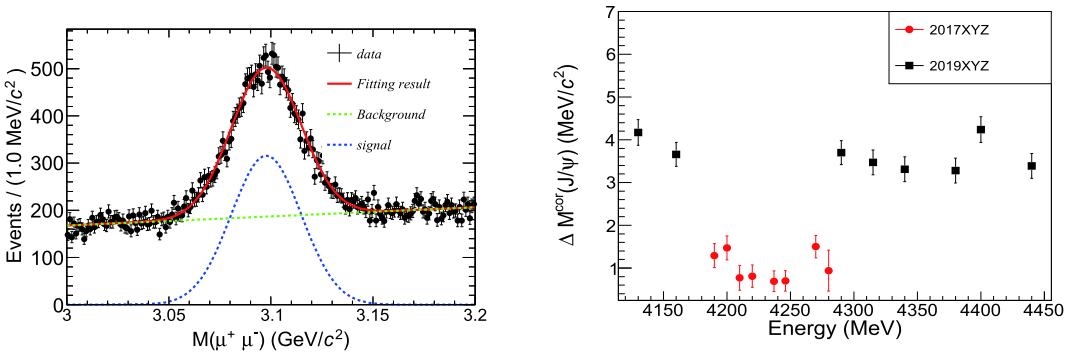

(a) (b)

Fig. 3. (color online) (a) Fit to the $M(\mu^+\mu^-)$ distribution in the J/ψ signal region for the 4190 data sample. Black dots with error bars are data, the red curve shows the fit result, the blue curve indicates the signal, and the green dashed line indicates the background. (b) The difference between $M^{\rm cor}(J/\psi)$ and the world average mass of J/ψ [16], $\Delta M^{\rm cor}(J/\psi)$ for each data sample.

muon track momentum calibration, as shown in Fig. 3(b). It can be seen that the bias in the J/ψ invariant mass is stable throughout one running year, but is quite different in the 2017XYZ and 2019XYZ samples. This may indicate that the calibrations in these two periods of time have significant differences.

Through MC simulation we find that the bias in the $M_{\rm p}(\mu^+\mu^-)$ measurement depends linearly on $M(\mu^+\mu^-)$ (see Fig. 4), and there exists $E_{\rm cm} = M(\mu^+\mu^-)$ with no radiation, so the correction to the $M_{\rm p}(\mu^+\mu^-)$ due to calibration is expressed as

$$\Delta M_{\rm cal} = -(k\times(E_{\rm cm}-m_{J/\psi})+\Delta M^{\rm cor}(J/\psi))({\rm MeV}), \quad (2)$$

where the slopes $k=(7.11\pm0.50)\times10^{-4}$ and $(7.04\pm0.57)\times10^{-4}$ correspond to the 2017XYZ and 2019XYZ samples, respectively. They agree within the statistical uncertainties of the MC samples, which indicates that the momentum dependence of the calibration constants is very similar in the 2017XYZ and 2019XYZ samples.

V. THE MASS SHIFT $\Delta M_{\rm ISR/FSR}$

$E_{\rm cm}$ of the initial e^+e^- pair is measured via the di-muon process $e^+e^-\to(\gamma_{\rm ISR/FSR})\mu^+\mu^-$. However, due to the emission of radiative photons, the invariant mass of the $\mu^+\mu^-$ pair is smaller than $E_{\rm cm}$ by $\Delta M_{\rm ISR/FSR}$. This correction is estimated with MC simulation using BABAYAGA3.5 [12].

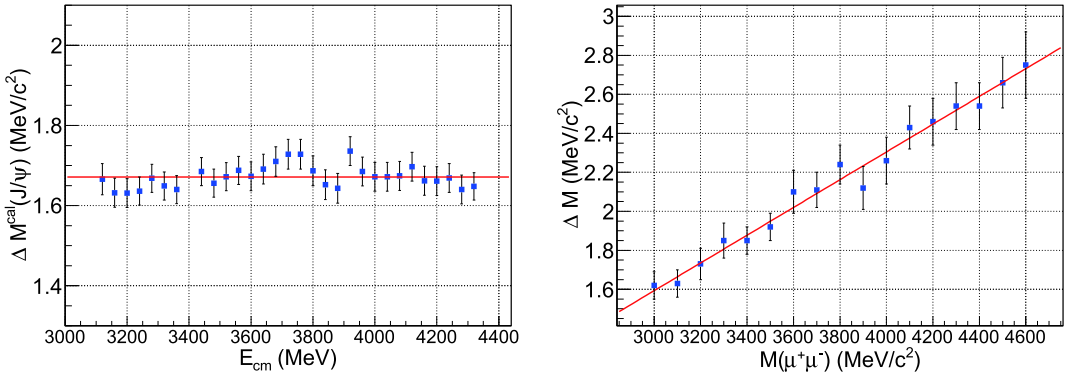

(a) (b)

Fig. 4. (color online) (a) The distribution of $\Delta M^{\rm cal}(J/\psi)$ of different $E_{\rm cm}$ for the MC simulation of $\gamma_{\rm ISR}J\psi$ process without FSR. The average value is 1.67 ± 0.01 MeV/c^2. (b) ΔM is the difference between the reconstructed and generated center-of-mass energy ($E_{\rm cm}$) reported as a function of $M(\mu^+\mu^-)$ ($M(\mu^+\mu^-)$ is equal to $E_{\rm cm}$ for events without radiation). The di-muon events are generated without radiation emission. The bias at J/ψ mass given from (b) is 1.67 ± 0.24 MeV/c^2, which is consistent with the result provided in (a). The linear fit to the points provides the dependence of the bias on $M_{\rm p}(\mu^+\mu^-)$ (slope k) due to track momentum calibration, which is assumed to be the same for data and simulation.

We generate one million di-muon events for each sample with ISR/FSR turned on or off, apply the same event selection criteria to the di-muon events as in the data (described in Sec. III), and fit the distributions of $M(\mu^+\mu^-)$ from the samples with ISR/FSR on and off with a Gaussian function in the range around the peak (same as in Sec. III). The difference in $M_{\rm p}(\mu^+\mu^-)$ is taken as the mass shift $\Delta M_{\rm ISR/FSR}$ caused by ISR or FSR. $\Delta M_{\rm ISR/FSR}$ versus $E_{\rm cm}$ shown in Fig. 5 indicates that the ISR/FSR effect depends linearly on $E_{\rm cm}$. The data are fitted with a linear function to provide an improved precision measurement of the correction. From the fit,

$$\Delta M_{\rm ISR/FSR} = (1.17\pm0.05)\times10^{-3}\times E_{\rm cm}+(-1.91\pm0.20)({\rm MeV}) \quad (3)$$

with a correlation factor of −0.99 between the slope and the intercept, and the goodness of the fit is $\chi^2/ndf = 6.2/12$.

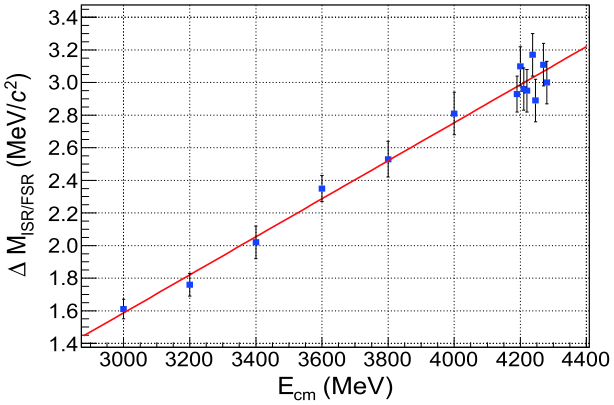

Fig. 5. (color online) Mass shift $\Delta M_{\rm ISR/FSR}$ versus CM energy for $e^+e^-\to(\gamma_{\rm ISR/FSR})\mu^+\mu^-$ MC samples. The solid red line is the linear fit.

VI. SYSTEMATIC UNCERTAINTIES

The systematic uncertainty in $E_{\rm cm}$ is from the momentum calibration of $\mu^\pm$, the estimation of the mass shift $\Delta M_{\rm ISR/FSR}$ due to ISR/FSR, the open angle cut of $\cos\theta_{\mu^+\mu^-}$, the corresponding fit procedure, and the generator. The bias of the momentum measurement of $\mu^\pm$ and the estimation of the mass shift $\Delta M_{\rm ISR/FSR}$ due to ISR/FSR both have a linear relationship with $E_{\rm cm}$, and the uncertainty produced by the uncertainty of the parameters is regarded as the systematic uncertainties.

To reduce the influence of the events with high radiation, we required $\cos\theta_{\mu^+\mu^-}<-0.9997$. Different cut values will give different $M_{\rm p}(\mu^+\mu^-)$ and corresponding radiation correction values $\Delta M_{\rm ISR/FSR}$. The changes in these two parts cancel each other out. The largest difference comes from the data between −0.9997 and −0.99975, and is 0.12 ± 0.02 MeV. We take 0.14 MeV as the uncertainty due to this requirement.

$M_{\rm p}(\mu^+\mu^-)$ is measured by fitting with a Gaussian function in the range of $(-1\sigma, +1.5\sigma)$ around the peak with fit quality $\chi^2/ndf<2.0$. If the fit range is smaller than the standard range, the difference in the fit results is less than 0.1 MeV. We take this as the uncertainty due to the fit method.

The contribution to the systematic uncertainty of the ISR/FSR correction from the generator is negligibly small, as claimed in Ref. [12]. The uncertainties from other sources, such as background and other event selection criteria, are negligible.

Assuming all sources of systematic uncertainty are independent, the total systematic uncertainty is obtained by

adding all the items in quadrature, which is listed in Table 1. The uncertainty is smaller than 0.6 MeV for all data samples.

VII. SUMMARY

The center-of-mass energies, $E_{\rm cm}$, of the data samples are obtained using Eq. (1), with the correction factors in Eqs. (2) and (3). The final results are listed in Table 1, including the statistical and systematic uncertainties. The corresponding statistical uncertainty is very small, and the systematic uncertainty is less than 0.36 MeV everywhere, with the exception of the point at 4280 MeV, where the error on $\Delta M^{\rm cor}$ is much larger than the rest. The stability of $E_{\rm cm}$ over time for the data samples is also examined.

The results presented in this work are essential for the discovery of new states and the investigation of the transitions of charmonium and charmoniumlike states [18] using the BESIII data. Some of the analyses have been presented in Refs. [19-24].

ACKNOWLEDGEMENTS

The BESIII collaboration thanks the staff of BEPCII and the IHEP computing center for their strong support.

References

[1] M. Ablikim *et al*. (BESIII Collaboration), Nucl. Instrum. Meth. A **614**, 345 (2010)
[2] D. M. Asner *et al*., Int. J. Mod. Phys. A **24**, 499 (2009)
[3] C. H. Yu *et al*., *Proceedings of IPAC2016*, Busan, Korea, 2016, doi:10.18429/JACoW-IPAC2016-TUYA01
[4] M. Ablikim *et al*. (BESIII Collaboration), Chin. Phys. C **44**, 040001 (2020)
[5] E. V. Abakumova *et al*., Nucl. Instrum. Meth. A **659**, 21 (2011)
[6] M. Ablikim *et al*. (BESIII Collaboration), Chin. Phys. C **40**, 063001 (2016)
[7] X. Li *et al*., Radiat. Detect. Technol. Methods **1**, 13 (2017)
[8] Y. X. Guo *et al*., Radiat. Detect. Technol. Methods **1**, 15 (2017)
[9] P. Cao *et al*., Nucl. Instrum. Meth. A **953**, 163053 (2020)
[10] Yifan Yang, *The Study of M1 Transitions of Charmonia at BESIII*, Ph.D thesis, Institute of High Energy Physics, 2019 http://www.irgrid.ac.cn/handle/1471x/2539883?mode=full
[11] S. Agostinelli *et al*. (GEANT4 Collaboration), Nucl. Instrum. Meth. A **506**, 250 (2003)
[12] G. Balossini, C. M. Carloni Calame, G. Montagna *et al*., Nucl. Phys. B **758**, 227 (2006)
[13] S. Jadach, B. F. L. Ward, and Z. Was, Phys. Rev. D **63**, 113009 (2001)
[14] S. Jadach, B. F. L. Ward, and Z. Was, Comput. Phys. Commun. **130**, 260 (2000)
[15] T. Skwarnicki *et al*., Report No. DESY F31-86-02 1986 (unpublished)
[16] P. A. Zyla *et al*. (Particle Data Group), Theor. Exp. Phys. **2020**, 083C01 (2020)
[17] E. Barberio and Z. Was, Comput. Phys. Commun. **79**, 291 (1994)
[18] N. Brambilla, S. Eidelman, C. Hanhart *et al*., Phys. Rept. **873**, 1-154 (2020), arXiv:1907.07583[hep-ex]
[19] M. Ablikim *et al*. (BESIII Collaboration), arXiv: 2004.13788 [hep-ex]
[20] M. Ablikim *et al*. (BESIII Collaboration), Phys. Rev. Lett. **124**, 242001 (2020)
[21] M. Ablikim *et al*. (BESIII Collaboration), Phys. Rev. D **101**, 012008 (2020)
[22] M. Ablikim *et al*. (BESIII Collaboration), Phys. Rev. Lett. **122**, 232002 (2019)
[23] M. Ablikim *et al*. (BESIII Collaboration), Phys. Rev. D **99**, 091103 (2019)
[24] M. Ablikim *et al*. (BESIII Collaboration), Phys. Rev. Lett. **122**, 202001 (2019)